HHS Public Access

Author manuscript

Exp Eye Res. Author manuscript; available in PMC 2023 January 01.

Published in final edited form as:

Exp Eye Res. 2022 January ; 214: 108884. doi:10.1016/j.exer.2021.108884.

RNA sequencing uncovers alterations in corneal endothelial metabolism, pump and barrier functions of *Slc4a11* KO mice

Diego G. Ogando, **Joseph A. Bonanno***

Vision Science Program, School of Optometry, Indiana University, Bloomington, IN 47405

Abstract

Slc4a11 KO mice show significant corneal edema, altered endothelial morphology, and mitochondrial ROS at an early age without a decrease in endothelial cell density. We examined the differential gene expression profile between wild type (WT) and KO with the goal of finding pathways related to corneal endothelial metabolic, pump and barrier function that can explain the corneal edema. Freshly dissected Corneal Endothelium-Descemet's Membrane (CEDM) and cultured Mouse Corneal Endothelial Cells (MCEC) were obtained from WT and *Slc4a11* KO mice. RNA sequencing Ingenuity Pathway Analysis (IPA) predicted activation, inhibition or differential regulation of several pathways. QPCR and Western analysis validated downregulation of Glycolytic enzymes, Mitochondrial complex components and Ion transporters. Functional testing revealed decreases in endothelial lactate production, Extracellular Acidification Rate (ECAR), glutaminolysis, and Oxygen Consumption Rate (OCR) of KO CEDM in the presence of Glutamine (Gln) that was not compensated by fatty acid oxidation. Stromal lactate was significantly elevated in KO along with decreased expression of MCT1 and MCT4 lactate transporters in endothelial cells. ATP levels were 2x higher in KO CEDM, concomitant with a 3-fold decrease in Na-K-ATPase activity and reduced basolateral membrane localization. Genes for cholesterol biosynthesis, glutathione metabolism and tight and adherens junctions were elevated. Alteration of tight junction structure and cortical cytoskeleton is evident in KO corneal endothelium with a significant increase in trans-endothelial fluorescein permeability. We conclude that *Slc4a11* KO induces a coordinated decrease in glycolysis, glutaminolysis, lactate transport and Na-K-ATPase activity. These changes together with an altered barrier function cause an accumulation of stromal lactate in Slc4a11 KO mice leading to chronic corneal edema.

Graphical Abstract

*Corresponding author Joseph A. Bonanno jbonanno@indiana.edu, School of Optometry, Indiana University, 800 E. Atwater Ave., Bloomington, IN 47405.

Author contributions

DGO and JAB designed the research plan, interpreted results, wrote and edited the manuscript. DGO performed all experiments.

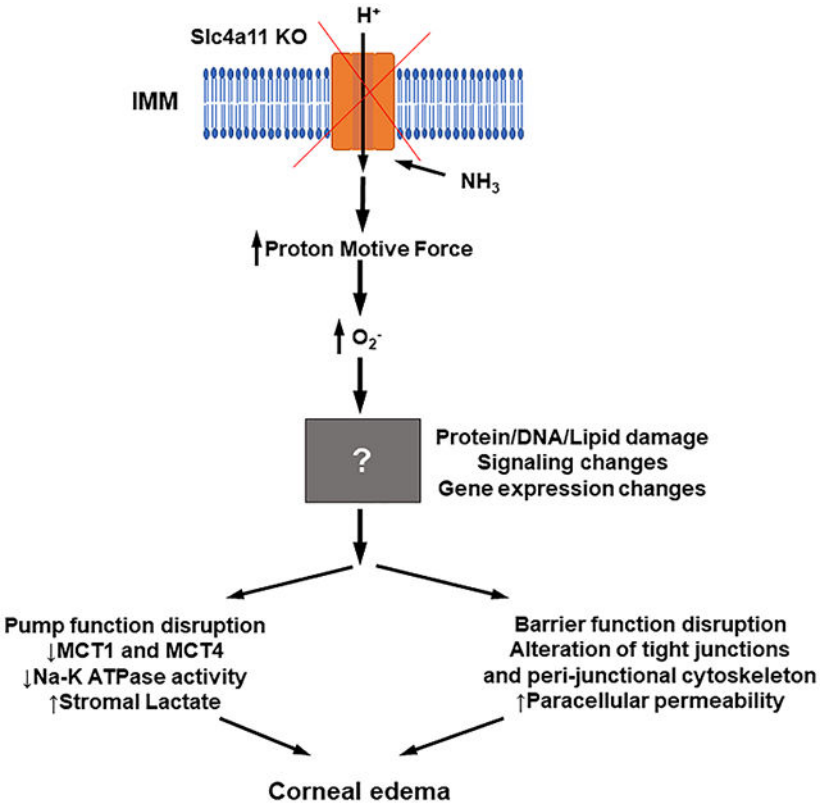

- *Slc4a11* KO removes mitochondrial uncoupling leading to an increase in the proton motive force resulting in increased O_2- (superoxide) production.
- Reactive Oxygen Species (ROS) induces the activation or inhibition of unknown transcription factors resulting in altered gene expression.
- *Slc4a11* KO causes decreased expression and activity of MCT1, MCT4 and b2 subunit of the Na^+K^+-ATPase. The consequence is impaired pump function leading in increased stromal Lactate accumulation.
- Moreover, the barrier function is disrupted by alteration of tight junctions and peri-junctional cytoskeleton that results in increased paracellular permeability.
- These changes combined result in corneal edema.

Keywords

RNA sequencing; corneal endothelial dystrophy; metabolism; Na-K-ATPase; barrier function; oxidative stress; lactate transporters

1. Introduction

CHED (Congenital Hereditary Endothelial Dystrophy) is due to homozygous and compound heterozygous mutations in *SLC4A11* (Vithana et al., 2006). In CHED, corneal endothelial cell loss and edema are apparent in childhood (Jiao et al., 2007). *Slc4a11* KO mice closely resemble CHED showing substantial corneal edema at early age (< 12 weeks) without

a decrease of endothelial cell density (Han et al., 2013; Li et al., 2020). Pump function is altered in this model as there is an age dependent increase in thickness of the cornea with concomitant stromal lactate accumulation (Li et al., 2020). At later ages, there is a significant reduction in cell density likely due to higher reactive oxygen species (ROS) production and oxidative damage in the KO (Han et al., 2013; Li et al., 2020; Ogando et al., 2019; Zhang et al., 2017a).

Slc4a11 is an ammonia-activated voltage driven H^+ transporter (Kao et al., 2020; Myers et al., 2016; Zhang et al., 2015). In corneal endothelium Slc4a11 is present in the basolateral membrane, mitochondrial inner membrane and possibly other cytoplasmic locations (Alka and Casey, 2018; Kao et al., 2016; Ogando et al., 2019). Function on the basolateral membrane is unclear. As an electrogenic H^+ transporter, it has been suggested that Slc4a11 activity could balance intracellular pH possibly facilitating Lactate:H^+ cotransport (Nehrke, 2016). On the mitochondrial inner membrane, Slc4a11 is an NH_3-sensitive uncoupler that reduces mitochondrial oxidative stress associated with glutamine catabolism (Ogando et al., 2019). Cells lacking Slc4a11 have higher proton motive force resulting in increased O_2- production and mitochondrial damage. Cell lines derived from *Slc4a11* KO mice have decreased glutaminolysis (Zhang et al., 2017b), secondary to increased Glutamine induced toxicity.(Ogando et al., 2019). Drugs that reduce oxidative stress such as the mitochondrial ROS quencher MitoQ, the mitochondrial uncoupler BAM15, and inhibitors of glutaminolysis protect KO cells and inhibit progression of corneal edema (Ogando et al., 2019; Shyam et al., 2021). A comparative transcriptome analysis of *Slc4a11* knockdown in cultured human primary corneal endothelial cells and Slc4a1$^{-/-}$ mouse corneal endothelial cells showed a global metabolic inhibition and reduced expression of ion transporters (Zhang et al., 2020).

In this study we avoided potential cell culture induced artifacts by performing a comparative transcriptome analysis of Corneal endothelium-Descemet's membrane (CEDM) samples from WT and KO mice to find differentially regulated pathways associated with metabolic, pump and barrier function. In *Slc4a11* KO CE tissue we observed a decrease in glycolysis, glutaminolysis, oxygen consumption, lactate transport and Na-K-ATPase activity. These changes together with an altered barrier function cause an accumulation of stromal lactate in *Slc4a11* KO mice leading to chronic corneal edema.

2. Materials and Methods

2.1. Mice

Slc4a11$^{-/-}$ mice (Han et al., 2013) were originally obtained from Eranga N. Vithana, Singapore Eye Research. All mice were housed, maintained, and used according to animal use policies of Indiana University, National Institutes of Health, US Department of Agriculture, and ARVO (the Association for Research in Vision and Ophthalmology) Statement on the Use of Animals in Ophthalmic and Vision Research.

2.2. Cells

Slc4a11$^{+/+}$ and Slc4a11$^{-/-}$ MCEC (mouse corneal endothelial cells) cell lines were generated and cultured as described previously (Zhang et al., 2017b). Briefly, CEDM was peeled from tsTAg/Slc4a11 $^{+/+}$ and tsTAg/Slc4a11$^{-/-}$ mice and incubated at 37°C for 15 minutes in OPTIMEM containing 2 mg/ml of Collagenase A (#10103578001, Sigma-Aldrich) 15 % FBS-HI and 1X antibiotics. (Zhang et al., 2017b). Cells were resuspended in Complete Media: OptiMEM (#51985, Thermo Fisher Scientific), that contains 14 mM Glucose and 4 mM L-Alanyl-Glutamine, 8% FBS-HI (#10082139, Thermo Fisher Scientific), 5 ng/ml EGF (#01-107 Millipore), 100 μg/ml pituitary extract (13026-14, Gibco), 200 mg/ml calcium cholide, chondroitin sulfate 0.8% (G6737, Sigma-Aldrich), 50 μg/ml gentamycin (#15710072, Thermo Fisher Scientific), antibiotic/antimycotic 1:100 (#15240062, Thermo Fisher Scientific) and 44 units/ml IFN-γ (#485-MI, R&D Systems); and cultured in FNC-coated 24 well-plates for ~12 days at 33 °C changing media every other day. Cell lines were used in passages 5-7 andwere passed in 0.5% trypsin-EDTA and cultured on FNC-coated wells. For experiments, cells were seeded in 12-well plates and cultured to near confluence at 33 °C in presence of IFN-γ and then switched to 37°C in the absence of IFN-γ for 3 days. At this point cells were cultured in Assay Medium: DMEM (no glucose, no glutamine, no sodium pyruvate, no phenol red) (#A14430-01, Thermo Fisher Scientific) supplemented with 5.5 mM glucose, 0.5 mM glutamine and dialyzed FBS 4% (#26400-036, Thermo Fisher Scientific).

2.3. Total RNA isolation from CEDM

RNA isolation from freshly dissected corneal endothelium-Descemet's membrane samples was essentially as described previously (Ogando et al., 2021). To obtain one sample, six CEDM peelings from three mice were pooled. Five WT and five KO samples were subjected to RNA sequencing. Integrity and concentration of RNA was determined using an Agilent TapeStation.

2.4. RNA Sequencing of total RNA

The RNA sequencing protocol with TruSeq Stranded mRNA kit was performed as previously described (Ogando et al., 2021). Following cDNA synthesis and adapter ligation, 12 cycles of PCR were performed to amplify the library. The FASTQ files and quantitative results can be obtained from the GEO DataSets database (accession number: GSE174586).

2.5. Ingenuity Pathway Analysis

Pathway analysis was performed with IPA software. The software first finds pathways that have significantly more regulated genes than expected by chance and assigns a P value. Then, the software analyses regulated genes in the pathway and makes predictions of activation or inhibition of the pathway. A Z-score is assigned, where positive values predict activation of the pathway and negative values predict inhibition.

Regulated pathways with no Z-score assigned (due to activators and inhibitors being regulated in similar proportion or due to insufficient data in the Knowledge Database of the software to make a confident prediction) were analyzed as well.

2.6. QPCR

Real-time PCR was performed as described previously (Ogando et al., 2021). To obtain one sample, six CEDM peelings from three mice were pooled. Three WT and three KO samples were subjected to QPCR. Supplementary Table lists per primers used.

2.7. Immunofluorescence

Immunofluorescence was performed as described previously (Ogando et al., 2021). Primary antibodies used: Mouse anti-ZO-1 (1:100) (Thermo Fisher Scientific #33-9100) and Rabbit anti-ATP1a1 (1:200) (Abcam #ab76020). Phalloidin-A488 (Thermo Fisher Scientific #A12379) 1X solution was used to stain F-actin.

2.8. Western Immunoassay

Western immunoassay using freshly dissected endothelium was performed as described previously (Ogando et al., 2021). Two CEDM peelings from one animal were pooled and lysed in RIPA 25 μl with PMSF 1 mM. Protein (1.5 μg, BCA determination) was loaded into a WES Protein Simple capillary electrophoresis module (Protein Simple, San Jose, CA USA) along with MCT1 (Santa Cruz Biotechnologies # sc-365501) 1:50, MCT2 (Santa Cruz Biotechnologies # sc-166925) 1:10, MCT4 (Ab Clonal #A10548) 1:10, Atp1a1 (Cell Signaling Technologies # 3010S) 1:10, α-Tubulin (Novus Biologicals #NB100-690) 1:10 antibodies and resulting electropherograms obtained.

2.9. Lactate Production

For lactate in tissue, individual CEDM were obtained and positioned in 96-well plates containing 100 μl of Bicarbonate-rich Ringers (BR) containing Gluc 5.5 mM + Gln 0.5 mM or Gluc 5.5 mM alone (n=4 for each group) and incubated for a total of 2 hours and 30 minutes at 37°C in a 5% CO_2 incubator. Every 30 minutes 10 μl aliquots were obtained and the same volume of fresh corresponding BR was replenished. At the end of the experiment CEDM was lysed in 35 μl of Lactate Assay Buffer (Biovision #K607). Lactate concentration in conditioned media and lysates was measured using a fluorescence assay (Biovision #K607) according to manufacturer instructions.

For lactate in cells, MCEC were seeded at 0.5 x 10^6 cells per well in 12-well format in complete medium. After one day cells were placed in 500 μl of BR containing Gluc 5.5 mM + Gln 0.5 mM or Gluc 5.5 mM alone (n=4 for each group) and incubated for a total of 2 hours and 30 minutes at 37°C in a 5% CO_2 incubator. Every 30 minutes aliquots of 50 μl were obtained and the same volume of fresh corresponding BR was replenished. At the end of the experiment CEDM was lysed in 70 μl of Lactate Assay Buffer. Lactate concentration in conditioned media and lysates was measured by the same kit indicated above. Protein was measured by BCA method.

2.10. Ammonia Production

Individual CEDM were obtained and positioned in 96-well plates containing 100 μl of Bicarbonate-rich Ringers (BR) containing Gluc 5.5 mM + Gln 0.5 mM or Gluc 5.5 mM alone (n=4 for each group) and incubated for a total of 24 hours. At different time points

20 μl aliquots were obtained and the same volume of fresh BR was replenished. At the end of the experiment CEDM was lysed in 30 μl of Ammonia Assay Buffer. Ammonia concentration in conditioned media and cell lysates was measured with a colorimetric kit (K370-100, Biovision). Protein lysate concentration was measured by BCA method.

2.11. Oxygen consumption and extracellular acidification Mito Stress Test

Corneas were obtained from WT and KO mice and CEDM was peeled (n=4 for each group). Four relaxing cuts were performed and CEDM was positioned endothelial side up on XF 24 Islet Capture Microplates (#101122-100, Agilent). CEDMs were incubated with XF DMEM Medium pH 7.4 containing Gluc 5.5 mM alone or plus Gln 1 mM for 45 minutes at 37°C (no CO_2). Tissue was subjected to the Seahorse XF Mito Stress test (#103015-100, Agilent) that included in sequence 30 μM Oligomycin, 20 μM FCCP, and lastly 30 μM Rotenone + 30 μM Antimycin. Protein concentration was obtained at the end for normalization. MCEC oxygen consumption conditions were previously described (Ogando et al., 2019). XF Long Chain Oxidation Mito Stress Test (103672-100, Agilent) was used for measuring palmitate oxidation with or without 4 μM Etomoxir (carnitine palmitoyltransferase-1 inhibitor). Results were normalized by cell number. ECAR (Extracellular acidification rates) under initial conditions (no inhibitors) were also obtained. OCR and ECAR data was analyzed by Seahorse Wave and Multi-File Report Generator Software.

2.12. ATP, Na/K ATPase activity, and Endothelial Permeability Assay

ATP bioluminescence assay using CEDM RIPA lysates (# A22066, Thermo Fisher scientific), ouabain sensitive Na^+-K^+ ATPase activity (#K417-100, Biovision) from sonicated CEDM supernatant depleted of phosphate with PiBind resin (#501-0015, Innova Biosciences) , and endothelial fluorescein permeability assay in WT and KO corneas (n=4 samples for each group) were performed as previously described (Ogando et al., 2021).

2.13. Statistical analysis

The n for each experiment was ≥3. Data is presented as Mean ± SEM. GraphPad Prism 9.0 (GraphPad Software, Inc.) was used for analysis. For comparing two groups Student's t-test was performed. For three or more groups, One-way or Two-way ANOVA was performed followed by Tukey's multiple comparison test. $p<0.05$ was considered significant.

3. Results

3.1. Regulated pathways associated with Slc4a11 Absence

Transcriptome comparison of corneal endothelium from twelve-week old *Slc4a11* KO and WT mice was studied by RNA-Seq. The principal component analysis shows that WT and KO samples clustered separately (Figure 1A). The analysis showed increased expression in 806 genes in KO as compared to WT with at least a 50% fold change (FC>1.5) whereas there was decreased expression of 644 genes (FC<−1.5, Figure 1B & 1C). Figure 1D shows the top 10 upregulated and downregulated genes. Pathway analysis found significant regulation of 89 pathways (Appendix Table A1). The analysis predicted activation of 31 pathways (Z>0), inhibition of 17 pathways (Z<0) and neither activation or inhibition of 7 pathways (Z=0) (Methods and Table A1). We selected some metabolic pathways and

pathways known to be involved in endothelial dystrophies (Figure 1E). Figure 1E left panel shows that Cholesterol Biosynthesis, P53 signaling, Actin Cytoskeleton Signaling, TGF-β Signaling and cAMP-mediated signaling pathways are predicted to be activated whereas Calcium Signaling, AMPK Signaling, Gluconeogenesis and Glycolysis are predicted to be inactivated. There were 34 significantly regulated pathways with no Z-score assigned, i.e. a mix of up and downregulated genes within the pathway (Methods and Table A1). From those we highlight two: Tight Junction Signaling and Epithelial Adherens Junction signaling (Figure 1E right panel).

Quantitative PCR analysis was performed for several pathways (Figure 2) validating increased expression of cholesterol synthesis enzymes, decreased expression of glycolytic enzymes, downregulation of OXPHOS components, and upregulation of Glutathione (GSH) metabolism enzymes. Overall, these data suggest that there is a significant depression of metabolism in *Slc4a11* KO corneal endothelium, which is consistent with previous reports (Ogando et al., 2019; Zhang et al., 2020; Zhang et al., 2017a) . The increase in GSH capacity may be related to increased oxidative stress seen in the KO (Guha et al., 2017; Ogando et al., 2019; Zhang et al., 2017a; Zhang et al., 2017b). We also see a decrease in MCT4 (Lactate:H^+ cotransporter), which is possibly coordinated with the depression in glycolytic enzyme expression. Junctional proteins Ocln, Cdh1, Cldn1, Cldn3, Cldn4, Tjp3, Tubb4a, Myh2 and Myh8 were upregulated whereas Rasd2 and Actn2 were downregulated. Lastly, Atp1b2, a component of the Na-K-ATPase is downregulated indicating a potential change in activity.

3.2. Metabolic alterations in Slc4a11 KO CE

Since corneal endothelial cells utilize both glucose and glutamine (Zhang et al., 2017a; Zhang et al., 2017b) we examined metabolism with both. Consistent with decreased expression of glycolytic enzymes in KO CEDM, lactate production is decreased with respect to WT in the presence of Glucose + Gln (Figure 3A). The lactate released from CEDM in the presence of Glucose only, does not differ between WT and KO. In WT, Gln increases lactate release vs Glucose only, however in KO, Gln decreases lactate release vs Glucose only; indicating that Gln stimulates lactate production in WT and has an inhibitory effect on glycolysis in KO CEDM (Figure 3A). Consistent with these differences in lactate release, Figure 3B shows that intracellular lactate concentrations of WT were increased in Gln while in KO CEDM there was no change and KO was significantly lower than WT. Accordingly, Extracellular Acidification Rate (ECAR) of WT and KO CEDM is similar in glucose only, but dropped considerably in KO in the presence of Gln (Figure 3C).

In MCEC cell lines that were developed from these mice (Zhang et al., 2017b), lactate release of KO is lower than WT, irrespective of the presence of Gln (Figure 3D) and intracellular Lactate in KO MCEC is significantly lower (Figure 3E). Gln does not have the same stimulatory effect on lactate production in the cultured cells as seen in fresh CEDM. However, Gln increases ECAR in MCEC WT, but not in KO (Figure 3F).

Glutaminolysis, as measured by ammonia production, is significantly decreased in KO CEDM with respect to WT (Figure 4A-B) similar to that previously observed with *Slc4a11* KO MCEC (Ogando et al., 2019; Zhang et al., 2017a; Zhang et al., 2017b). Consistent

with facilitation of glutamine metabolism by Slc4a11, Oxygen Consumption Rates (OCR) in WT corneal endothelial tissue in the presence of glutamine is higher than KO (Basal, ATP production, Maximal Respiration and Spare Respiratory Capacity) (Figure 4C-D). WT cells have higher proton leak than KO in the presence of Gln as expected for a NH_3-activated mitochondrial uncoupler. In KO CEDM, Gln does not increase OCR, consistent with decreased glutamine catabolism (Figure 4C-D).

Since glycolysis and glutaminolysis are decreased in KO vs WT we asked if fatty acid oxidation is increased to compensate the metabolic deficit. Figure 5 shows that in WT MCEC OCR increased significantly with palmitate and was partially inhibited by Etomoxir (carnitine palmitoyltransferase-1 inhibitor). Conversely, KO MCEC did not significantly oxidize palmitate, indicating that in KO cells fatty acid oxidation is dysfunctional and does not compensate for the deficit in glycolysis and glutaminolysis.

3.3. Pump and barrier function disruption in Slc4a11 KO CE

Changes in metabolic enzymes, lactate transport, and Na-K-ATPase expression were examined more closely in relation to the failure of the endothelial pump seen in the KO animals (Han et al., 2013; Li et al., 2020). Figure 6 confirms a decrease in the protein levels of lactate:H^+ cotransporter MCT4 and Na-K-ATPase subunit ATP1b2, whereas Na-K-ATPase α1 subunit levels were not affected. Interestingly, whereas mRNA levels were not affected, we also see decreased expression of MCT1, suggesting translational regulation. As such, the low expression of these lactate transporters parallels the decrease in metabolic activity in KO CEDM (Figure 3 and 4). These findings suggest that there may be a deficit in ATP availability. Figure 6B shows that the resting [ATP] was approximately 3-fold higher in the KO. However, Figure 6C shows that Na^+ K^+-ATPase activity was about 3-fold lower in the KO. Moreover, immunofluorescence of Na-K-ATPase α1 showed a decreased level of staining and disorganized expression in the basolateral membrane of KO corneal endothelium (Figure 6D and E). This disorganization is also reflected in the alteration of tight junctions (ZO1) and cortical cytoskeleton associated with adherens junctions (F-actin) in KO (Figure 7A). Along with the disorganization of lateral membranes there was increased fluorescein permeability of KO CEDM indicating that barrier function is diminished (Figure 7B).

4. Discussion

Slc4a11 KO recapitulates CHED (Han et al., 2013), showing significant corneal edema at very early age. Here we show differential gene expression of several pathways that shed light on the origin of the corneal edema. The *Slc4a11* KO mouse corneal endothelium showed decreased expression of components of glycolysis, lactate transport, mitochondria, the Na-K-ATPase, and cell junctions. Conversely, upregulation of other junctional components was uncovered along with cholesterol biosynthesis and glutathione production. Examining the functional consequences of these changes more closely, we found decreases in lactate production, MCT lactate transporter expression, Na-K-ATPase activity, and diminished endothelial barrier function. The reduction in lactate transport capacity and dysfunctional permeability barrier of the endothelium together can explain pump failure,

since they are all needed for proper functioning of the endothelial pump (Li et al., 2016), and is consistent with previous data showing accumulation of stromal lactate concomitant with corneal edema (Li et al., 2020; Ogando et al., 2021).

Slc4a11 codes for a membrane transporter that is in the basolateral membrane (Jalimarada et al., 2013; Vilas et al., 2013), the inner mitochondrial membrane (Ogando et al., 2019), and possibly other membrane locations of corneal endothelial cells (Kao et al., 2016). Slc4a11 is an electrogenic H^+ transporter, i.e. H^+ influx driven by negative membrane potential, that is activated by ammonia (Zhang et al., 2015) and possibly high pH (Kao et al., 2020; Quade et al., 2020). Previous studies showed altered glutaminolysis, mitochondrial function, ROS production, and oxidative damage in Slc4a11$^{-/-}$ cells (Ogando et al., 2019; Zhang et al., 2020; Zhang et al., 2017a). Therefore, it was not surprising to find similar changes directly within the in vivo tissue. We found downregulation of the expression of components of the respiratory chain consistent with decreased oxygen consumption in the presence of Gln (Figure 4C&D) and decreased glutaminolysis (Figures 4A&B). Surprisingly, glycolysis was activated in WT CE tissue in the presence of Gln (Figure 3A-C), whereas in KO tissue Gln had a suppressive effect as evidenced by a reduced ECAR and lactate efflux. One possible explanation for glutamine dependent increase in lactate production is that more pyruvate is shunted to lactate in the presence of glutamine because glutaminolysis reduces glucose dependent oxidation within the TCA cycle (Zhang et al., 2017b), i.e. ATP production from mitochondrial glutaminolysis offsets the need to oxidize pyruvate so it is shunted to lactate. This does not happen in the *Slc4a11* KO because glutaminolysis is suppressed with increased ROS production and as we show here, there is downregulation of glycolytic activity.

Deficient glutaminolysis in the *Slc4a11* KO is due to mitochondrial damage from oxidative stress. Slc4a11 acts as an ammonia sensitive mitochondrial uncoupler that prevents run away mitochondrial membrane potential hyperpolarization during glutamine fed activation of the TCA cycle and the electron transport chain (Ogando et al., 2019). The mechanism for the dramatic change in gene expression seen here in the *Slc4a11* KO is unknown. Oxidative stress and mitochondrial disruption are likely triggers for signal transduction events that culminate in this pattern of metabolic and cell junctional changes. For example, it is known in retina that oxidative stress inhibits glycolysis (Hegde et al., 2010). A recent study showed that induction of *Slc4a11* KO produced corneal edema within 2 weeks (Ogando et al., 2021), suggesting that the effect on gene expression is fast and not the result of a slow chronic deterioration. Reactive oxygen species activate the master antioxidant transcription factor NRF2 leading to increased expression of various antioxidant enzymes including those for the production of glutathione (Figure 2). Interestingly, Slc4a11 expression is increased by oxidative stress through an NRF2 dependent mechanism (Guha et al., 2017; Guha and Roy, 2021), consistent with Slc4a11 being a modulator of ROS. Whereas reducing oxidative stress in the *Slc4a11* KO mouse can rescue the phenotype (Ogando et al., 2019; Shyam et al., 2021), additional studies are needed to understand the mechanisms leading to the differences in gene expression.

Even though metabolic pathways are diminished in KO cells (Ogando et al., 2021; Zhang et al., 2020), ATP levels are higher than in WT; as observed as well in the inducible

KO model (Ogando et al., 2021). In the CEDM of the conventional KO, we found downregulated expression of the Atp1b2 Na-K-ATPase subunit (Figure 2), a 3-fold decrease in Na-K-ATPase activity (Figure 6C) and decreased and disorganized basolateral membrane expression in KO corneal endothelium (Figure 6D&E). The decreased metabolic activity of KO corneal endothelium suggests energy deficiency, however we found increased ATP levels in KO CEDM (Figure 6A). The metabolic deficit in the KO is not compensated by an increase in fatty acid oxidation (Figure 5). Interestingly, CE can oxidize palmitate, but this ability is lost in Slc4a11 KO. We postulate that the higher ATP level in KO CE is due to the low Na-K-ATPase activity found in KO as this enzyme is the major ATP consumer in the cell (Howarth et al., 2012).

Our results using fresh CEDM tissue are comparable to those found in a recent paper comparing gene expression of human primary corneal endothelial cell Slc4a11 knock down vs Ctrl and MCEC KO vs WT cell lines where a generalized decrease in metabolism is found in KO cells including glycolysis, glutaminolysis and TCA cycle and a decreased expression of ion transporters (Zhang et al., 2020). However, there are also some differences between CEDM tissue and cultured cells. In KO cell lines Zhang et al found downregulation of several ion transporters including NBCe1(Zhang et al., 2020), however we did not see an effect on NBCe1 in CEDM KO tissue. Mitochondrial dysfunction and lower OCR levels in the presence of Gln is observed in KO CEDM and cultured cells. However, the differences in OCR between WT and KO tissue are much smaller than in cell lines(Ogando et al., 2019). This may be explained by the high number of respiratory complex genes found to be downregulated in KO in vitro (Zhang et al., 2020) versus in vivo (Figure 2). In the current study we also found that cultured MCEC showed similar metabolic differences as WT and KO tissue, however Gln enhanced ECAR in WT MCEC but did not stimulate lactate production as seen in CEDM. Lastly, MCEC KO cells or Human KO cell lines have decreased levels of ATP compared to WT in the presence of glutamine (Ogando et al., 2019; Zhang et al., 2020), indicating differences in compensatory processes in vivo versus in vitro.

An intact osmotic barrier function is needed in order to couple lactate with water flux (Diamond and Bossert, 1967; Li et al., 2020). Whereas stromal lactate accumulation can occur by MCT knockdown (Li et al., 2014) or inhibition of the Na -K -ATPase alone (Li et al., 2016), we also found that adherens and tight junctions are disrupted with concomitant increase in paracellular permeability in KO CEDM (Figure 7). We observed downregulation of Actn2 in KO CE (Figure 2), which could contribute to barrier loss, since Actn2 can link Cadherins and the actin cytoskeleton. The upregulation of Claudins and other junctional genes (Figure 2) may represent an attempt to re-establish the barrier function as observed in intestinal epithelium after barrier compromise due to inflammation (Garcia-Hernandez et al., 2017). Interestingly, there was an upregulation of enzymes involved in cholesterol production in the KO. This could potentially have a role in the cell morphology changes by altering plasma membrane fluidity. The disruption of pump and barrier functions found here in the conventional Slc4a11 KO is consistent with that observed within 8 weeks of induced KO of Slc4a11 (Ogando et al., 2021).

In summary, *Slc4a11* KO induces a coordinated decrease in glycolysis, glutaminolysis, lactate transport and Na-K-ATPase activity. These changes together with an altered barrier

function cause an accumulation of stromal lactate in *Slc4a11* KO mice leading to chronic corneal edema. Reductions in ROS levels (Ogando et al., 2019; Shyam et al., 2021) can rescue the phenotype indicating that oxidative stress may be the trigger for the changes in gene expression.

Supplementary Material

Refer to Web version on PubMed Central for supplementary material.

Acknowledgements

We would like to thank Douglas B. Rusch and Aaron M. Buechlein from the Center for Genomics and Bioinformatics, Indiana University for expert technical assistance.

Supported by NIH R01EY031321 and R01EY008834 to JAB.

Abbreviations

CEDM	Corneal endothelium-Descemet's membrane
CE	Corneal endothelium
MCEC	Mouse corneal endothelial cells
ECAR	Extracellular acidification rate
OCR	Oxygen consumption rate
MCT1	Monocarboxylate Transporter 1
MCT4	Monocarboxylate Transporter 2
CHED	Congenital hereditary endothelial dystrophy
BR	Bicarbonate-rich Ringers
FC	Fold Change
FDR	False Discovery Rate

References

Alka K, Casey JR, 2018. Ophthalmic Nonsteroidal Anti-Inflammatory Drugs as a Therapy for Corneal Dystrophies Caused by SLC4A11 Mutation. Invest Ophthalmol Vis Sci 59, 4258–4267. [PubMed: 30140924]

Diamond JM, Bossert WH, 1967. Standing-gradient osmotic flow. A mechanism for coupling of water and solute transport in epithelia. J Gen Physiol 50, 2061–2083. [PubMed: 6066064]

Garcia-Hernandez V, Quiros M, Nusrat A, 2017. Intestinal epithelial claudins: expression and regulation in homeostasis and inflammation. Ann N Y Acad Sci 1397, 66–79. [PubMed: 28493289]

Guha S, Chaurasia S, Ramachandran C, Roy S, 2017. SLC4A11 depletion impairs NRF2 mediated antioxidant signaling and increases reactive oxygen species in human corneal endothelial cells during oxidative stress. Sci Rep 7, 4074. [PubMed: 28642546]

Guha S, Roy S, 2021. Enhanced expression of SLC4A11 by tert-Butylhydroquinone is mediated by direct binding of Nrf2 to the promoter of SLC4A11. Free Radic Biol Med 167, 299–306. [PubMed: 33744340]

Han SB, Ang HP, Poh R, Chaurasia SS, Peh G, Liu J, Tan DT, Vithana EN, Mehta JS, 2013. Mice with a targeted disruption of Slc4a11 model the progressive corneal changes of congenital hereditary endothelial dystrophy. Invest Ophthalmol Vis Sci 54, 6179–6189. [PubMed: 23942972]

Hegde KR, Kovtun S, Varma SD, 2010. Inhibition of glycolysis in the retina by oxidative stress: prevention by pyruvate. Mol Cell Biochem 343, 101–105. [PubMed: 20559692]

Howarth C, Gleeson P, Attwell D, 2012. Updated energy budgets for neural computation in the neocortex and cerebellum. J Cereb Blood Flow Metab 32, 1222–1232. [PubMed: 22434069]

Jalimarada SS, Ogando DG, Vithana EN, Bonanno JA, 2013. Ion transport function of SLC4A11 in corneal endothelium. Invest Ophthalmol Vis Sci 54, 4330–4340. [PubMed: 23745003]

Jiao X, Sultana A, Garg P, Ramamurthy B, Vemuganti GK, Gangopadhyay N, Hejtmancik JF, Kannabiran C, 2007. Autosomal recessive corneal endothelial dystrophy (CHED2) is associated with mutations in SLC4A11. J Med Genet 44, 64–68. [PubMed: 16825429]

Kao L, Azimov R, Shao XM, Abuladze N, Newman D, Zhekova H, Noskov S, Pushkin A, Kurtz I, 2020. SLC4A11 function: evidence for H(+)(OH(-)) and NH3-H(+) transport. Am J Physiol Cell Physiol 318, C392–C405. [PubMed: 31774702]

Kao L, Azimov R, Shao XM, Frausto RF, Abuladze N, Newman D, Aldave AJ, Kurtz I, 2016. Multifunctional ion transport properties of human SLC4A11: comparison of the SLC4A11-B and SLC4A11-C variants. Am J Physiol Cell Physiol 311, C820–C830. [PubMed: 27581649]

Li S, Kim E, Bonanno JA, 2016. Fluid transport by the cornea endothelium is dependent on buffering lactic acid efflux. Am J Physiol Cell Physiol 311, C116–126. [PubMed: 27225657]

Li S, Kim E, Ogando DG, Bonanno JA, 2020. Corneal Endothelial Pump Coupling to Lactic Acid Efflux in the Rabbit and Mouse. Invest Ophthalmol Vis Sci 61, 7.

Li S, Nguyen TT, Bonanno JA, 2014. CD147 required for corneal endothelial lactate transport. Invest Ophthalmol Vis Sci 55, 4673–4681. [PubMed: 24970254]

Myers EJ, Marshall A, Jennings ML, Parker MD, 2016. Mouse Slc4a11 expressed in Xenopus oocytes is an ideally selective H+/OH− conductance pathway that is stimulated by rises in intracellular and extracellular pH. Am J Physiol Cell Physiol 311, C945–C959. [PubMed: 27681179]

Nehrke K, 2016. H(OH), H(OH), H(OH): a holiday perspective. Focus on "Mouse Slc4a11 expressed in Xenopus oocytes is an ideally selective H+/OH− conductance pathway that is stimulated by rises in intracellular and extracellular pH". Am J Physiol Cell Physiol 311, C942–C944. [PubMed: 27784681]

Ogando DG, Choi M, Shyam R, Li S, Bonanno JA, 2019. Ammonia sensitive SLC4A11 mitochondrial uncoupling reduces glutamine induced oxidative stress. Redox Biol 26, 101260. [PubMed: 31254733]

Ogando DG, Shyam R, Kim ET, Wang YC, Liu CY, Bonanno JA, 2021. Inducible Slc4a11 Knockout Triggers Corneal Edema Through Perturbation of Corneal Endothelial Pump. Invest Ophthalmol Vis Sci 62, 28.

Quade BN, Marshall A, Parker MD, 2020. pH dependence of the Slc4a11-mediated H(+) conductance is influenced by intracellular lysine residues and modified by disease-linked mutations. Am J Physiol Cell Physiol 319, C359–C370. [PubMed: 32520610]

Shyam R, Ogando DG, Choi M, Liton PB, Bonanno JA, 2021. Mitochondrial ROS Induced Lysosomal Dysfunction and Autophagy Impairment in an Animal Model of Congenital Hereditary Endothelial Dystrophy. Invest Ophthalmol Vis Sci 62, 15.

Vilas GL, Loganathan SK, Liu J, Riau AK, Young JD, Mehta JS, Vithana EN, Casey JR, 2013. Transmembrane water-flux through SLC4A11: a route defective in genetic corneal diseases. Hum Mol Genet 22, 4579–4590. [PubMed: 23813972]

Vithana EN, Morgan P, Sundaresan P, Ebenezer ND, Tan DT, Mohamed MD, Anand S, Khine KO, Venkataraman D, Yong VH, Salto-Tellez M, Venkatraman A, Guo K, Hemadevi B, Srinivasan M, Prajna V, Khine M, Casey JR, Inglehearn CF, Aung T, 2006. Mutations in sodium-borate cotransporter SLC4A11 cause recessive congenital hereditary endothelial dystrophy (CHED2). Nat Genet 38, 755–757. [PubMed: 16767101]

Zhang W, Frausto R, Chung DD, Griffis CG, Kao L, Chen A, Azimov R, Sampath AP, Kurtz I, Aldave AJ, 2020. Energy Shortage in Human and Mouse Models of SLC4A11-Associated Corneal Endothelial Dystrophies. Invest Ophthalmol Vis Sci 61, 39.

Zhang W, Li H, Ogando DG, Li S, Feng M, Price FW Jr., Tennessen JM, Bonanno JA, 2017a. Glutaminolysis is Essential for Energy Production and Ion Transport in Human Corneal Endothelium. EBioMedicine 16, 292–301. [PubMed: 28117276]

Zhang W, Ogando DG, Bonanno JA, Obukhov AG, 2015. Human SLC4A11 Is a Novel NH3/H+ Co-transporter. J Biol Chem 290, 16894–16905. [PubMed: 26018076]

Zhang W, Ogando DG, Kim ET, Choi MJ, Li H, Tenessen JM, Bonanno JA, 2017b. Conditionally Immortal Slc4a11−/− Mouse Corneal Endothelial Cell Line Recapitulates Disrupted Glutaminolysis Seen in Slc4a11−/− Mouse Model. Invest Ophthalmol Vis Sci 58, 3723–3731. [PubMed: 28738416]

Highlights

- RNA sequencing comparing transcriptome expression of mouse corneal endothelium of *Slc4a11* KO vs WT mice reveals regulation of several pathways associated with corneal endothelial function.
- *Slc4a11* KO Mouse corneal endothelium *in vivo* shows decreased glycolysis, glutaminolysis, and oxygen consumption in the presence of glutamine.
- Failure of the corneal endothelial pump is evident as lactate accumulates in the stroma. This failure is explained by decreased activity of Na-K-ATPase and downregulation of lactate^{-}: H^{+} cotransporters MCT1 and MCT4.
- Barrier function is perturbed as paracellular permeability is increased and structure of tight junctions and peri-junctional cytoskeleton is altered.

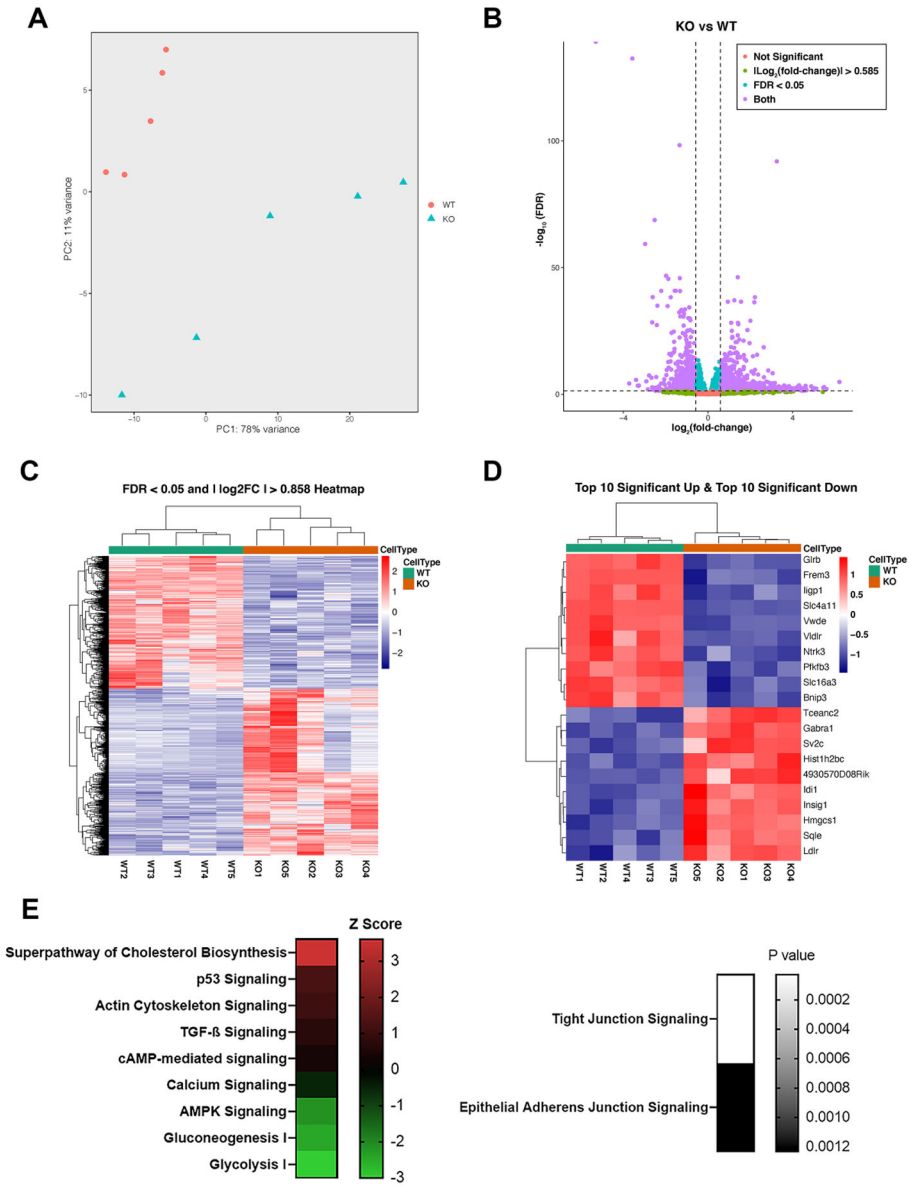

Figure 1. RNA sequencing of CEDM from Slc4a11 WT and KO uncovers differential expression of genes and regulated pathways.

A. Principal component analysis of five WT and five KO samples. **B.** Volcano plot showing regulated genes with FDR<0.05 (-Log_{10}FDR>1.3) and [Log_2 FC]>0.585 ([FC]>1.5). FC: Fold Change expression KO/WT. FDR: False Discovery Rate. Purple dots: Genes with [FC]>1.5 and FDR<0.05. Cyan dots: Genes with [FC]<1.5 and FDR<0.05. Light green dots: Genes with [FC]>1.5 and FDR>0.05. Orange dots: Genes with [FC]<1.5 and FDR>0.05. **C.** Heatmap of all regulated genes with FDR<0.05 and [Log_2 FC]>0.858. **D**. Heatmap of top 10 up or downregulated genes with FDR<0.05 and [Log_2 FC]>0.585. **E**. Left panel. Selected regulated IPA Canonical Pathways arranged by Z score. Red indicates activated prediction (Z>0) and green inhibited prediction (Z<0). Z score reference gradient score is shown on the right. Right panel. Two regulated pathways with no Z-score arranged by P value. P value reference gradient is shown on the right.

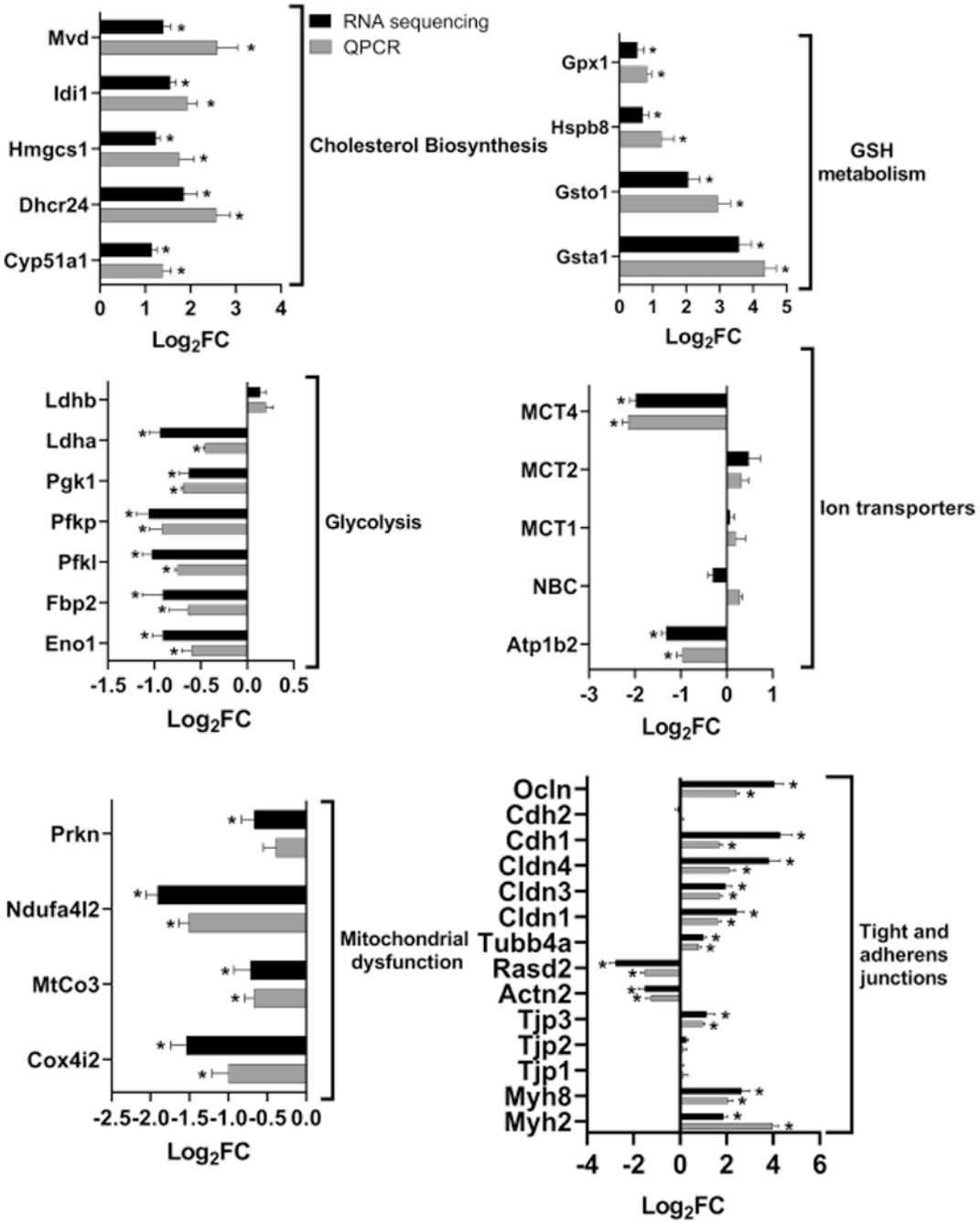

Figure 2. QPCR validation of gene regulation observed in RNA sequencing.

QPCR validation of regulated genes for selected pathways. For QPCR, n=3, for RNA sequencing, n=5. *p<0.05, significantly different from zero.

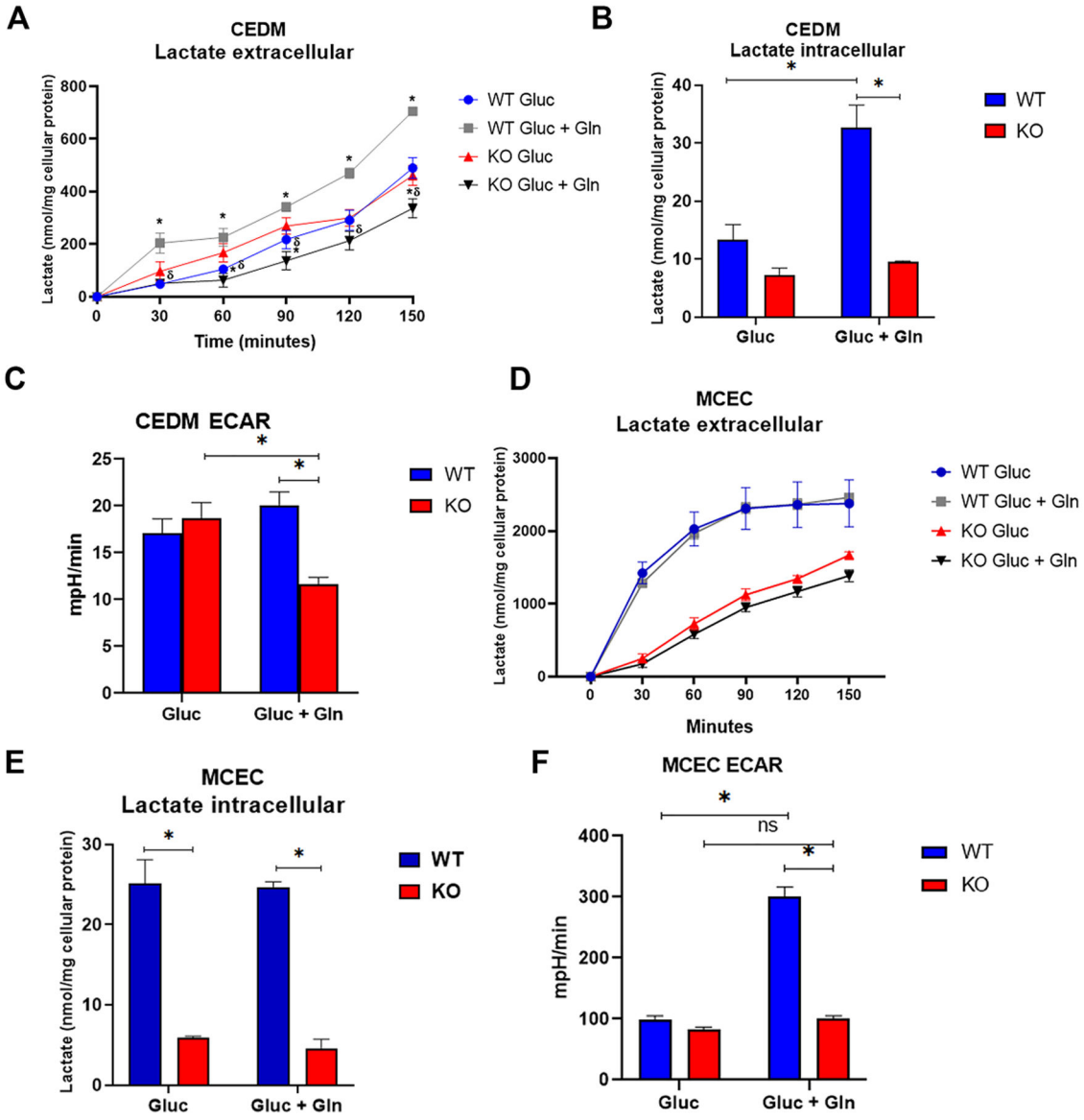

Figure 3. Decreased glycolysis in CEDM KO in presence of Gln.

A. Ex-vivo lactate efflux from CEDM vs time. *: p<0.05 vs KO Gluc + Gln, n=4. **B.** CEDM intracellular lactate concentration measured at the end of the incubation. *: p<0.05, n=4. **C.** CEDM basal Extracellular Acidification Rate (ECAR). *: p<0.05, n=4. **D.** MCEC lactate extracellular production vs time,n=4. **E.** MCEC intracellular lactate concentration measured at the end of the incubation. *: p<0.05, n=4. **F**. MCEC ECAR p<0.05, n=4.

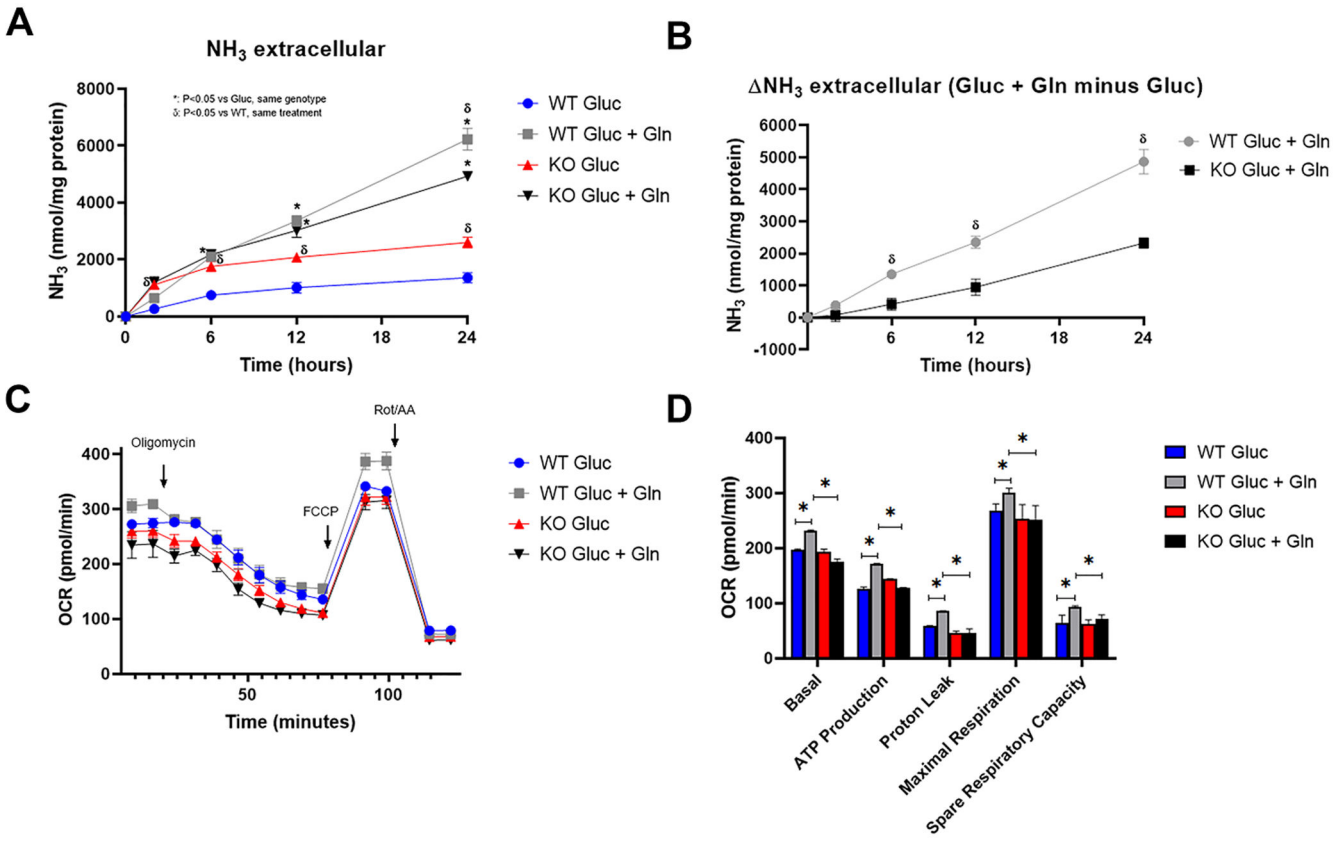

Figure 4. KO CEDM has decreased glutaminolysis and OCR in presence of Gln.

A. CEDM extracellular NH_3 production. *: $p<0.05$ vs Gluc, same genotype, δ: $p<0.05$ vs WT, same treatment, n=4. **B**. Ammonia production attributable to glutamine. ΔNH_3 extracellular (Gluc + Gln minus Gluc). δ:$p<0.05$ vs KO. **C.** OCR Mito Stress Test of CEDM. n=4. **D.** OCR parameters *: $p<0.05$, n=4.

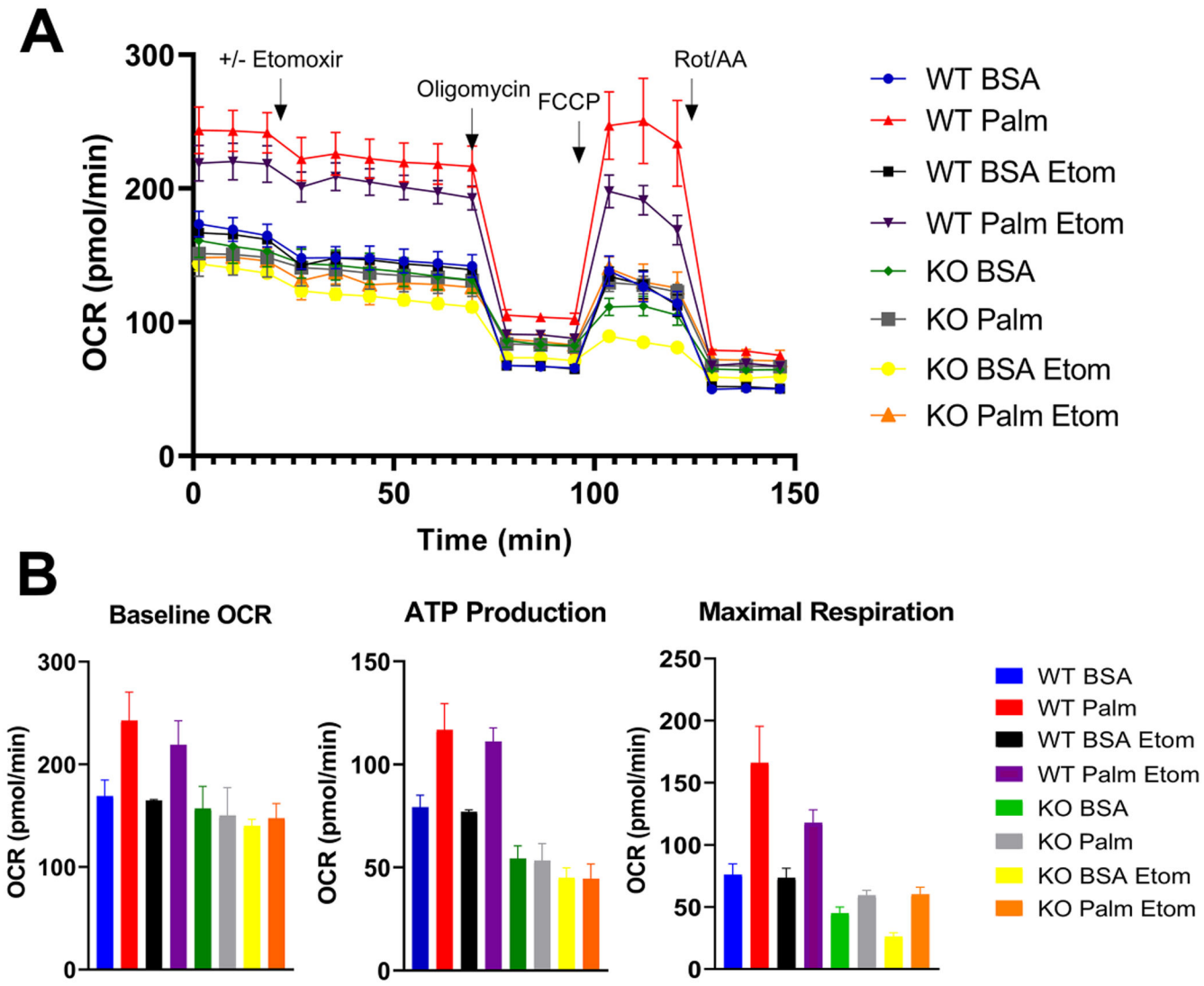

Figure 5. A. Fatty acid oxidation is not increased in MCEC KO vs WT.

A. OCR Mito Stress Test of MCEC ± Palmitate ± Etomoxir (carnitine palmitoyltransferase-1 inhibitor), n=4. **B.** OCR parameters. n=4, BSA (bovine serum albumin).

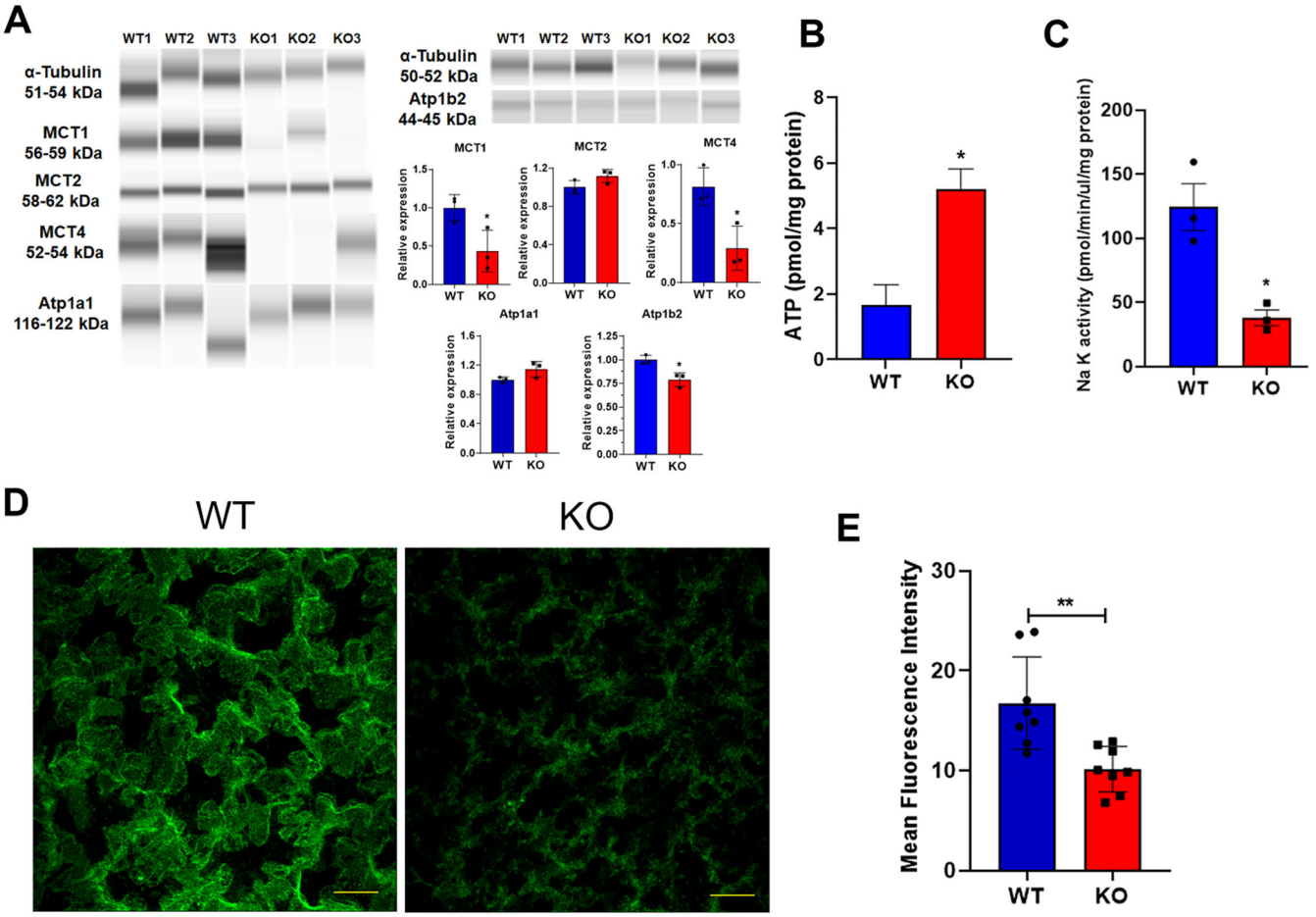

Figure 6. Decreased Na-K-ATPase activity and decreased MCT1 and MCT4 expression in CEDM KO.

A. Protein Wes blot of MCT1, MCT2, MCT4, Atp1a1, Atp1b2 and housekeeping protein α-Tubulin and quantification. *: $p<0.05$, n=4. **B.** CEDM ATP content at 12 weeks of age. *: $p<0.05$, n=3. **C.** Na-K-ATPase activity of CEDM at 12 weeks of age. *: $p<0.05$, n=4. **D.** Immunofluorescence of Atp1a1 of WT and KO CE tissue at 12 weeks of age. Bar: 10 μm. **E.** Fluorescence quantification of Atp1a1. **: $p<0.01$, n=4.

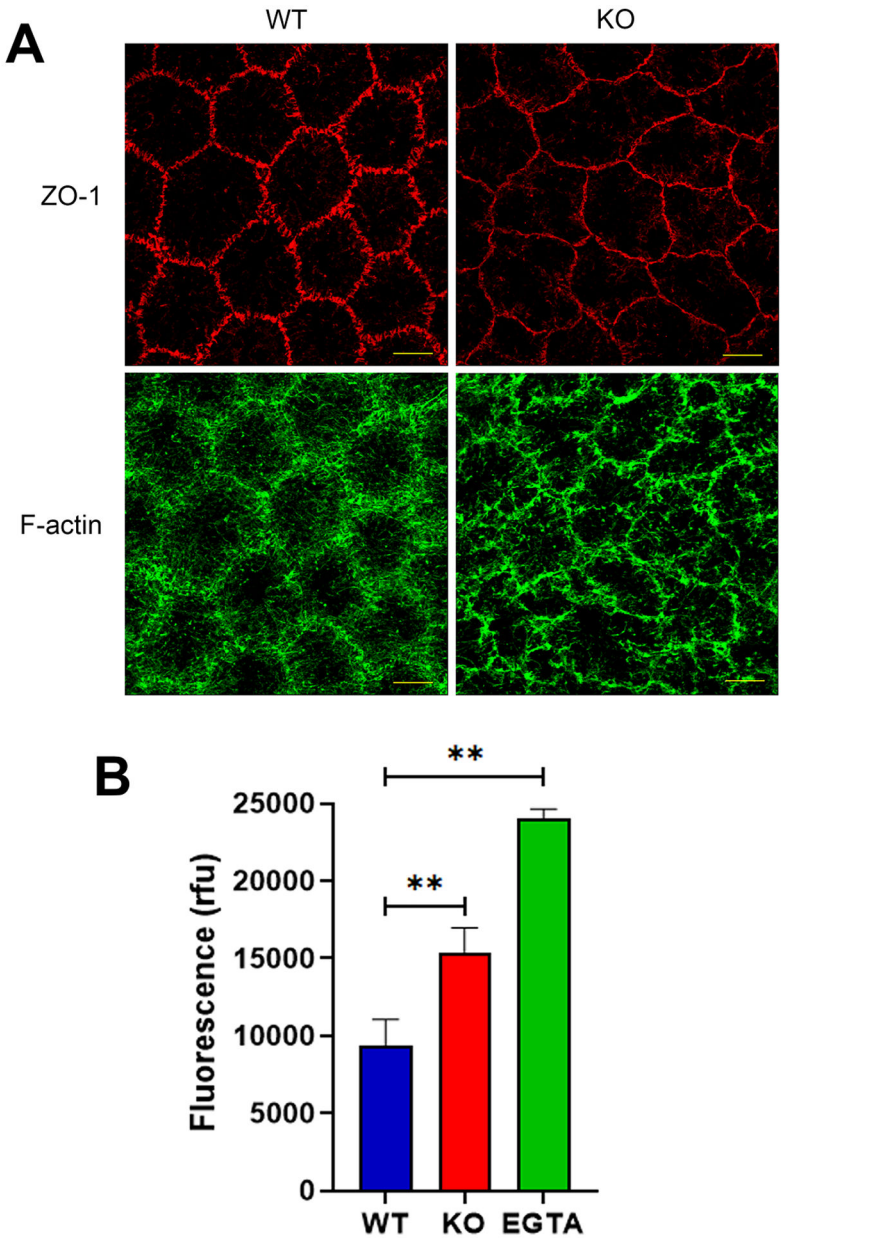

Figure 7. Effect of *Slc4a11* KO on Endothelial Morphology.

A. Immunofluorescence of ZO-1 (Red) and F-actin with Phalloidin (Green) of WT and KO CE tissue at 12 weeks of age. Bar: 10 μm. **B**. Paracellular permeability of corneal endothelium to fluorescein measured in WT and KO corneas at 12 weeks of age. **: $p<0.01$, n=4.